Journal of Solid State Chemistry 182 (2009) 3021–3030

Contents lists available at ScienceDirect

Journal of Solid State Chemistry

journal homepage: www.elsevier.com/locate/jssc

2,4,6-Trimethylpyridinium perchlorate: Polar properties and correlations with molecular structure of organic–inorganic hybrid crystal

M. Wojtaś [a,*], A. Gągor [b], O. Czupiński [a], A. Pietraszko [b], R. Jakubas [a]

[a] Faculty of Chemistry, University of Wrocław, Joliot–Curie 14, 50–383 Wrocław, Poland
[b] W. Trzebiatowski Institute of Low Temperature and Structure Research PAS, P.O. box 1410, 50–950 Wrocław, Poland

ARTICLE INFO

Article history:
Received 3 April 2009
Received in revised form
17 July 2009
Accepted 26 July 2009
Available online 5 August 2009

Keywords:
Perchlorate
Phase transition
X-ray
Dielectric
Pyroelectric

ABSTRACT

$[(CH_3)_3C_5H_2NH][ClO_4]$ has been synthesized and characterized by X-ray (at 344, 245, 180 and 115K), calorimetric, dilatometric, dielectric and pyroelectric measurements. At room temperature the crystal structure is polar, space group $Pmn2_1$. It consists of discrete disordered $[ClO_4]^-$ anions and ordered trimethylpyridinium cations giving the 3D network of hydrogen bonds. The compound reveals a rich polymorphism in the solid state. It undergoes four solid–solid phase transitions: from phases I to II at 356/327K (heating/cooling), II→III at 346/326, III→IV at 226K and IV→V at 182/170K. $[(CH_3)_3C_5H_2NH][ClO_4]$ reveals a strong pyroelectric response over a wide temperature region (phases III, IV and V) with the spontaneous polarization changes (ΔP_s) of the order of $1.5-8\times10^{-3}\,C/m^2$. The spontaneous polarization is irreversible over all the polar phases, however, the magnitude of the ΔP_s in the vicinity of the phase transitions is characteristic of compounds with the ferroelectric order. The molecular mechanism of the successive phases transitions in the studied crystal is proposed.

1. Introduction

Noncentrosymmetric bulk materials are usually characterized by interesting physical properties, such as pyroelectricity, piezoelectricity, ferroelectricity, nonlinear optical second harmonic generation (SHG) [1–17]. Among these properties, ferroelectric behavior is the most important and useful, and it is of great interest. Ferroelectric materials find applications in electric-optical devices, information storage, switchable NLO (nonlinear optical) devices, and light modulators [18]. A special attention is focused on the synthesis of hybrid class of inorganic–organic materials because of their interesting architectures and wide variety of physical properties. Organic substructure of these compounds is usually responsible for their molecular hyperpolarizability, electric permittivity and spontaneous polarization. The inorganic part determines thermal and mechanical stability of the crystals. The combination of these various features attributed to both organic and inorganic substructures may lead to an excellent ferroelectric and NLO materials with large macroscopic permittivities [19–24].

The molecular-ionic connections of heteroaromatic pyridinium cations with tetrahedral anions like BF_4^-, ClO_4^-, ReO_4^-, IO_4^- and FSO_3^- are interesting examples of inorganic–organic hybrid materials showing ferroelectric properties [25], and references therein. Both ionic sublattices of these salts were found to be highly disordered in the paraelectric phases. The polar aromatic cations usually perform reorientational motion about the pseudo-hexagonal axis of the aromatic ring. Slowing down this motion and partial ordering of the dipolar moieties in the respective mesophases lead to an appearance of long-range dipole ordering of ferroelectric type. Recently, a novel imidazolium ferroelectrics as a simple 1:1 salts, $[C_3N_2H_5][ClO_4]$ and $[C_3N_2H_5][BF_4]$ have been synthesized [26,27]. In contrast to the pyridinium complexes, in the case of imidazolium analogs, the ferroelectric properties originate predominantly from the behavior of distorted tetrahedral fluoroborate and perchlorate anions.

In search of new polar materials we extended our studies to tetrafluoroborate and perchlorate connections containing substituted pyridinium cations bestowed with a permament dipole moment like: aminopyridinium—$[4-NH_2PyH][ClO_4]$ [28] and $[4-NH_2PyH][BF_4]$ [29], cyanopyridinium: $[2-CNC_5H_4NH][ClO_4]$, $[(4-CNC_5H_4NH)][ClO_4]\cdot H_2O$ [30,31]. The interactions of cations with the monovalent tetrahedral counter anions (e.g. $[ClO_4]^-$, BF_4^-) were expected to create interesting dielectric properties of crystals. Both aminopyridinium analogues reveal structural phase transitions attributed to the dynamics of the organic cations. $[4-NH_2PyH][ClO_4]$ disclose ferroic (ferroelastic) and pyroelectric properties below 241K. The second derivative, $[4-NH_2PyH][BF_4]$, is characterized by a rich sequence of phase transitions (at 250, 281, 388 and 485K) and ferroic (ferroelastic) properties in the low-temperature phases. It was shown that all the phase transitions are due to the change in the dynamical state of the

* Corresponding author.
E-mail address: maciekwo@eto.wchuwr.pl (M. Wojtaś).

0022-4596/$ - see front matter © 2009 Elsevier Inc. All rights reserved.
doi:10.1016/j.jssc.2009.07.055

4-aminopyridinium and tetrafluoroborate or perchlorate moieties. No ferroelectric ordering in the case of aminopyridinium analogs was found. [2−CNC_5H_4NH][ClO_4] crystallizes in the piezoelectric space group ($P2_12_12_1$) and undergoes to the polar phase but the spontaneous polarization is irreversible. The phase transition to polar phase $P2_12_12_1 \rightarrow P2_1$ takes place at 170K, thus below that temperature the ferroelastic properties are expected.

An organic–inorganic hybrid material, simple ionic salt: 2,4,6-trimethylpyridinium perchlorate, [$(CH_3)_3C_5H_2NH$][ClO_4] has been synthesized. In this paper we report single-crystal X-ray, powder X-ray, calorimetric, dilatometric, dielectric and pyroelectric studies of this compound over a wide temperature range. A possible mechanism of the structural phase transitions in [$(CH_3)_3C_5H_2NH$][ClO_4] is discussed with particular attention focused on unusually strong pyroelectric properties.

2. Experimental

[$(CH_3)_3C_5H_2NH$][ClO_4] was obtained by adding 2,4,6-trimethylpyridine (98%, BOH laboratory reagents) to an aqueous solution of $HClO_4$ (70%, AppliChem). The compound was recrystallized twice from the solution and the single crystals were grown at constant room temperature by evaporation. Elemental analyses on C, H and N were (% exp./theor.): C(43.11/43.35), H(5.51/5.46), N(6.25/6.32). Monocrystals had a shape of a rectangular prism. The biggest face was perpendicular to the [10−1] and the smallest face was perpendicular to the [010] direction. The third face was oriented perpendicularly to the [101] direction. As grown crystal is shown in Fig. 1. The crystals of [$(CH_3)_3C_5H_2NH$][ClO_4] are optically transparent and non-hygroscopic.

Differential scanning calorimetry (DSC) was performed using a Perkin-Elmer DSC-7 in the temperature range 100-400K with scanning rates from 1 to 20K/min. The temperature of the phase transition was estimated by approximation to the scanning rate 0K/min.

The dilatometric measurements were made with a thermomechanical analyser, Perkin-Elmer TMA-7, over the temperature range 100–400K with a rate of 3K/min. The dimensions of the sample were of the order of $8 \times 3 \times 1\,mm^3$.

The spontaneous polarization was measured between 130 and 400K by a charge integration technique using a Keithley 617 Programmable Electrometer. The temperature was stabilized by temperature controller Instec STC200. The dimensions of the sample studied were of the order of $5 \times 3 \times 1\,mm^3$.

Dielectric measurements were performed by an HP 4285A Precision LCR Meter in the frequency range between 75kHz and 5MHz in the temperature range from 140 to 400K. The dimensions of the sample studied were of the order of $5 \times 3 \times 1\,mm^3$. The overall error was less than 5% and 10% for the real and imaginary parts of the complex electric permittivity, respectively.

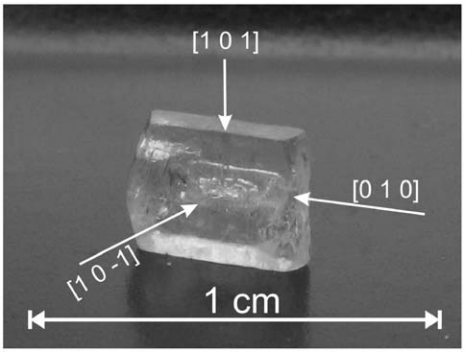

Fig. 1. The as-grown crystal of [$(CH_3)_3C_5H_2NH$][ClO_4].

A single crystal X-ray data collection was performed on a Kuma KM4CCD diffractometer with CCD data collector using Mo$K\alpha$ radiation. Small single-domain crystals were carefully selected, checked for twinning mounted with epoxy glue at the tip of quartz fibre and used for data collection at 115, 180, 210, 245, 258 and 295K. For the measurements at high temperatures the sample was put at the tip of quartz capillary to prevent the crystal from sublimation. Thermal evolution of lattice parameters was measured from 115 to 300K with a step of 10–15K. Lattice parameters were obtained by a least square fit to 110 reflections. An open flow nitrogen cryosystem (Oxford Cryosystem) was used for experiments from 300 to 115K, while a simple high temperature attachment with hot-air flow was used for the experiments at temperatures ranging between 300 and 344K.

The CrysAlis. software version 1.170.32 [32] was used for data processing. An empirical absorption correction was applied using spherical harmonics implemented in Scale3 Abspack scaling algorithm. The structure was solved by direct methods and refined by the full-matrix least-squares method by means of SHELX-97 program package [33]. The details of the crystal structure investigations at 115, 180, 210, 245, 258, 295 and 344K can be obtained from the CCDC data base. Table 1 summarizes the data collection, reduction and structure parameters at selected temperatures.

Powder diffraction data were collected on X'Pert PRO X-ray diffractometer with PIXcel ultra-fast line detector, focusing mirror and Soller slits for Cu$K\alpha$ radiation. The samples were measured in a glass capillaries of 0.7mm. The high-temperature measurements were done using Anton Paar 1200N High-Temperature Oven Chamber. The unit cell was found using program Dicvol implemented in Xpert High Score Plus.

3. Thermal analysis

Results of differential scanning calorimetry measurements are presented in Fig. 2. Starting from room temperature, on heating, compound undergoes two first-order phase transitions at 346K (PT III→II) and 356K (PT II→I). These transitions are manifested as two, well separated, peaks. Both thermal anomalies shift strongly ($\Delta T \approx 30\,K$) towards lower temperatures on cooling and are evidently overlapped. The values of the entropy on heating were 10.3 and $21.5\,J\,mol^{-1}\,K^{-1}$ for the III→II and II→I phase transformations, respectively. The values of the entropy of these transitions on cooling were estimated only roughly by fitting the DSC curve with two Gaussian curves. Approximate value of ΔS was $12\,J\,mol^{-1}\,K^{-1}$ for the (II→III) PT and $24\,J\,mol^{-1}\,K^{-1}$ for the (I→II) PT. Although ΔS values are burdened with significant error ($\pm 10-15\%$), the entropy magnitude shows that phase transitions mechanism may be classified as an order–disorder type.

Over the low temperature region the [$(CH_3)_3C_5H_2NH$][ClO_4] crystal experiences two phase transitions at 226/226K (PT III→IV) and 170/182K (PT IV→V), on cooling/heating. The first one is manifested only as the deflection of the baseline with lack of the temperature hysteresis what indicates the second-order character of this transformation. In turn, the second transformation is manifested as a peak ($\Delta S_{tr} = 1.3\,J\,mol^{-1}\,K^{-1}$) and exhibits the temperature hysteresis of the order of 12K what is typical of the first-order PT. It is worth noting that all phase transitions are well reversible and reproducible.

The phase transition situation is depicted in the following diagram:

$$\text{phase}: \ \mathrm{V} \underset{\text{cooling } 170\,K}{\overset{\text{heating } 182\,K}{\rightleftharpoons}} \mathrm{IV} \underset{226\,K}{\overset{226\,K}{\rightleftharpoons}} \mathrm{III} \underset{326\,K}{\overset{346\,K}{\rightleftharpoons}} \mathrm{II} \underset{327\,K}{\overset{356\,K}{\rightleftharpoons}} \mathrm{I}$$

Table 1
Crystal data, experimental details and structure refinement results for $[(CH_3)_3C_5H_2NH][ClO_4]$.

Crystal data				
Chemical formula	$[(CH_3)_3C_5H_2NH][ClO_4]$			
Phase, temperature (K)	III, 344	III, 245	IV, 180	V, 115
Cell setting, space group	Orthorhombic, $Pmn2_1$	Orthorhombic, $Pmn2_1$	Orthorhombic, $Pbn2_1$	Monoclinic, Pn
M_r, Z	221.64, 2	221.64, 2	221.64, 8	221.64, 2
a (Å)	9.3181(4)	9.2570(4)	9.1658(4)	9.1256(8)
b (Å)	5.1989(2)	5.0702(2)	20.0743(9)	5.0959(4)
c (Å)	11.0082(4)	10.9570(4)	10.8540(4)	10.8893(10), $\beta = 90.894(7)$
V (Å^3)	533.28(4)	514.27(4)	1997.1(2)	506.33(8)
D_x (Mg/m^3), μ (mm^{-1})	1.380, 0.348	1.431, 0.361	1.474, 0.371	1.454, 0.366
Crystal form, color	Rectangular prism, colorless			
Crystal size (mm)	$0.25 \times 0.24 \times 0.2$		$0.3 \times 0.25 \times 0.15$	
Data collection				
Data collection method	$\Delta\omega$ CCD camera			
Absorption correction	Multi-scan (based on symmetry-related measurements)			
T_{min}, T_{max}	0.887, 0.928	0.85, 0,95	0.85, 0.95	0.85, 0.95
No. of measured and observed reflections	5437, 1030	4701, 1126	18764, 1968	4537, 1802
Criterion for observed reflections	$I > 2\sigma(I)$			
R_{int}, Θmax (°)	0.025, 27.09	0.016, 28.27	0.05, 26.71	0.018, 26.37
Refinement				
Refinement on	F^2			
$R[F^2 > 2\sigma(F^2)]$, w$R(F^2)$, S	0.036, 0.045, 1.06	0.025, 0.057, 1.06	0.042, 0.109, 0.92	0.031, 0.083, 1.09
No. of reflections, param.	1239, 89	1195, 89	3588, 288	1832, 133
$\Delta\rho_{max}$, $\Delta\rho_{min}$ (e/Å^3)	0.196, −0.103	0.157, −0.107	0.221, −0.216	0.339, −0.266

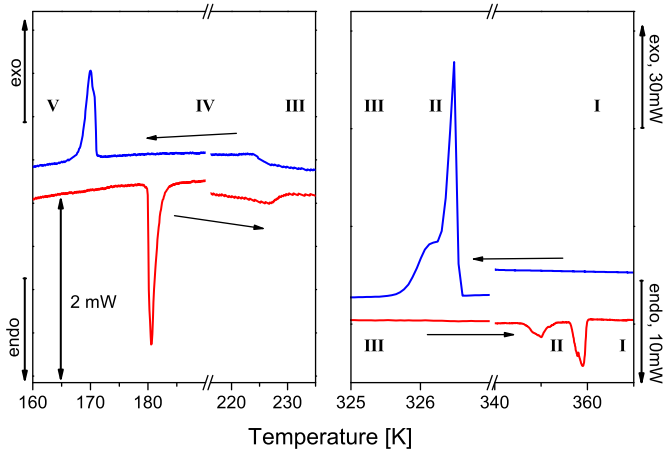

Fig. 2. DSC curves for the $[(CH_3)_3C_5H_2NH][ClO_4]$ crystal. Note that in order to make the right hand side picture more legible different scales were applied for cooling and heating runs. Arrows show directions of runs (cooling or heating).

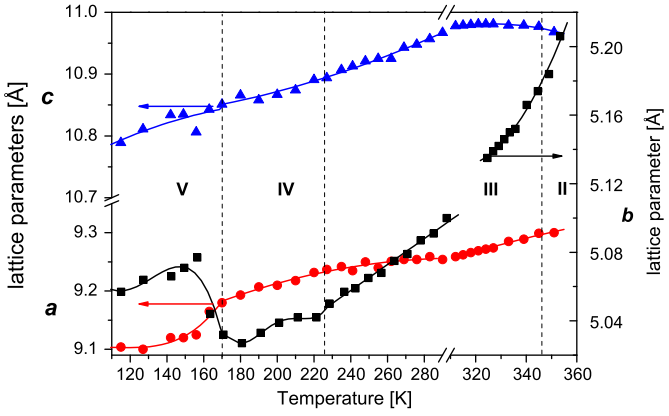

Fig. 3. Thermal evolution of lattice parameters in $[(CH_3)_3C_5H_2NH][ClO_4]$ on cooling. The a, b and c parameters are marked as red circles, black squares and blue triangles, respectively. Standard deviations are comparable to the points marked in the picture. The data are obtained from single crystal X-ray and powder X-ray measurements below and above room temperature, respectively. The lattice parameters are numbered using the cell choice of phase III. (For interpretation of the references to color in this figure legend, the reader is referred to the web version of this article.)

4. Crystal structure

4.1. Thermal evolution of lattice parameters

Thermal evolution of lattice parameters and diffraction peaks intensity corroborate the character of structure transformations disclosed by DSC. The values of lattice parameters, monoclinic β angle and volume of the unit cell vs. temperature are presented in Figs. 3 and 4, respectively. The data below room temperature (RT) were collected using single-crystal X-ray diffraction whereas above RT using powder X-ray diffraction. Powders were measured up to 390K. The structure transition from phase III to II leads to the change of the unit cell dimensions to $a = 7.565(5)$ Å, $b = 6.570(1)$ Å and $c = 4.638(4)$ Å. There is no direct transformation between the unit cell of phases III and II thus, the data concerning phases II and I are presented only in the text, see Section 4.2.

The III→IV PT does not entail a significant change of lattice parameters as expected for second-order PT. However, it manifests in the change of the intensity of Bragg peaks and appearance of additional satellite reflections. Fig. 5 shows the temperature induced intensity changes of $1\,2\,-6$ Bragg peak and its satellite $1\,2\,-6\,-1$ which arises from the unit cell quadrupling in the b direction.

IV→V PT is accompanied by an expansion of the crystal along the b direction by about 0.05Å and contraction along the a direction by about 0.045Å at the transition point that confirms its first-order character. The c parameter does not change significantly. Additionally, a monoclinic distortion appears due to the crystal system change. Below the IV→V PT the patterns that have originated in the unit cell quadrupling disappear and the cell returns to the dimensions from the phase III.

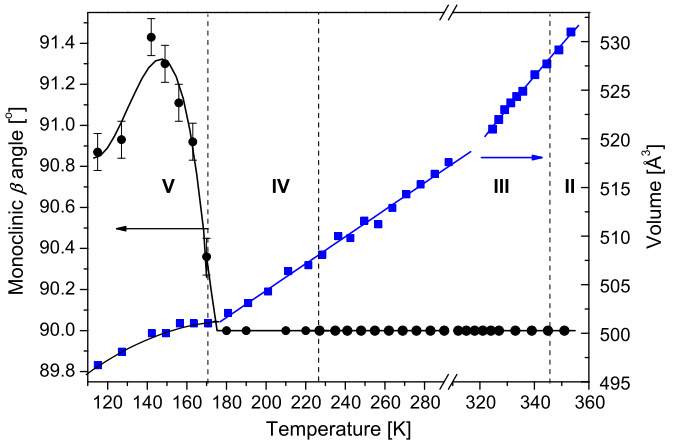

Fig. 4. The thermal evolution of unit cell volume (squares) and monoclinic β angle (circles) in $[(CH_3)_3C_5H_2NH][ClO_4]$ on cooling. Standard deviations for volume are comparable to the points marked in the picture. The volume data are obtained from single crystal X-ray and powder X-ray measurements below and above room temperature, respectively.

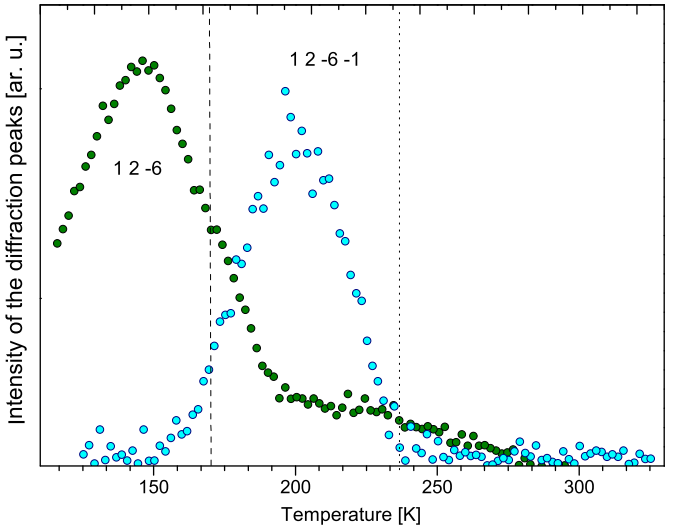

Fig. 5. Intensity of 12−6 Bragg and 12−6−1 satellite peaks in $[(CH_3)_3C_5H_2NH][ClO_4]$ on cooling.

The structure of the room temperature phase III was found to be orthorhombic with the $Pmn2_1$ space group suggested by systematic extinctions and averaging of reflection intensities. Since no important differences have been found between the structure at 245 and 344K the further discussion is based on the data from 245K. The phase transition from the phases III to IV is accompanied by quadrupling of the unit cell in *b* direction. The structure was solved in the non-standard setting $Pbn2_1$ of the group $Pna2_1$ to keep the cell choice of the phase III. The second phase transition from the phases IV to V is associated with symmetry decrease to monoclinic one. The structure was solved in non-standard setting *Pn* of *Pc* space group.

In all the phases positions of H atoms bound to N atoms were taken from difference-Fourier maps and refined with restraints, whereas the H atoms bound to the C atoms were included in geometric positions and treated as riding atoms.

4.2. High temperature phases I and II

Above 346K transparent single-crystalline samples convert to polycrystalline state keeping the morphology of single crystal.

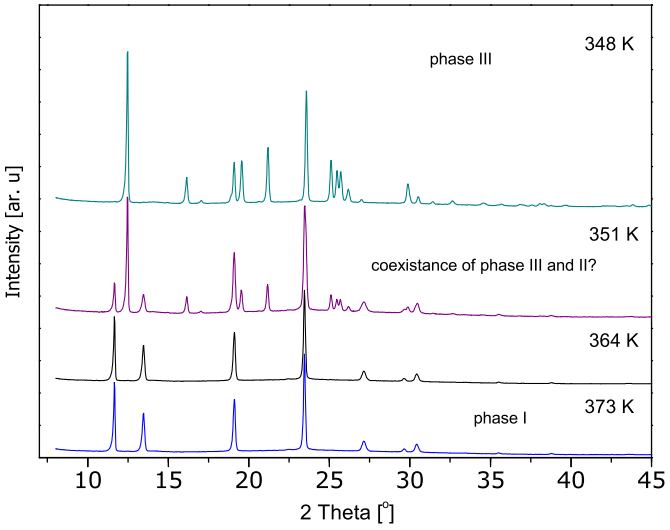

Fig. 6. Powder diagrams of $[(CH_3)_3C_5H_2NH][ClO_4]$ at high temperatures.

Thus, the transition from III to II phase results in crystal powdering suggesting the drastic changes of the crystal structure. Fig. 6 presents the powder diagrams of the $[(CH_3)_3C_5H_2NH][ClO_4]$ at 348, 351, 364 and 373K. The diagram at 348K is characteristic of the room temperature phase III. At 351K there is a coexistence of two phases and all the peaks can be indexed using two orthorhombic unit cells with $a = 9.300(5)$ Å, $b = 5.206(4)$ Å, $c = 10.968(4)$ Å, and $a' = 7.565(5)$ Å, $b' = 6.570(1)$ Å and $c' = 4.638(4)$ Å. The first one is typical for the phase III whereas using the second one we can index all diffraction peaks of the prototype phase I. There is no clear evidence of the phase II, however, it is possible that distinction between the II and I phase is not possible using X-RPD method. At 373K all peaks can be indexed in orthorhombic cell with parameters $a = 7.597(1)$ Å, $b = 6.581(1)$ Å and $c = 4.653(1)$ Å. The possible space groups which can be attributed to this cell choice are either non-polar *P*222 and *Pmmm* or polar *Pmm*2. None of them needs special reflection conditions. Attempts were made to solve the structure of prototype phase, unfortunately they failed mainly due to the lack of a direct transformation between the unit cell of phase III and unit cell of phase I as well as significant disorder which must be present in the structure at high temperatures.

4.3. Room temperature phase III

The $[(CH_3)_3C_5H_2NH][ClO_4]$ crystallizes in the orthorhombic system with the non-centrosymetric $Pmn2_1$ space group. The crystal structure is built up from $[(CH_3)_3C_5H_2NH]^+$ cations of C_s symmetry, with the mirror plane imposed on a N(1)–C(4)–C(41) axis, and disordered $[ClO_4]^-$ tetrahedra. Fig. 7 illustrates the $[(CH_3)_3C_5H_2NH][ClO_4]$ structure at 245K.

The $[ClO_4]^-$ is disordered over two different orientations in the 1:1 ratio about the (100) mirror plane passing through Cl and O(1) atoms. The site point-group symmetry C_s of Cl atom is higher than the molecular C_1 point group of $[ClO_4]^-$ introducing these two symmetry equivalent positions. The Cl–O distances, however, indicate rather slight distortion of the perchlorate anion from the tetrahedral symmetry. The shortest Cl–O bond equals to 1.407(2)Å, whereas the longest one to 1.429(2)Å, the angles vary from 107.40° to 110.96(11)°that are standard values for perchlorate ions [34,35]. The details of the geometry of the $[ClO_4]^-$ anion and $[(CH_3)_3C_5H_2NH]^+$ cation are listed in Tables 3 and 4 in supplementary materials.

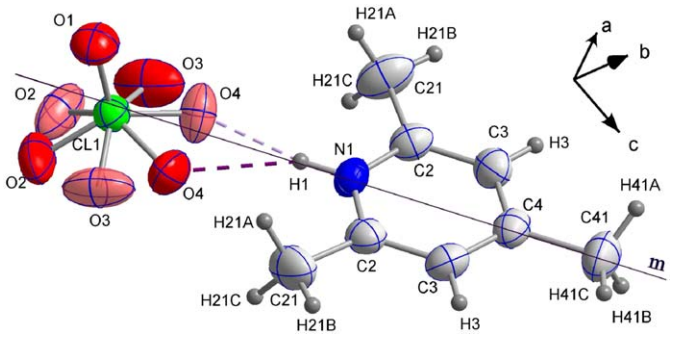

Fig. 7. The molecular structure along with the atom numbering scheme in phase III, 245K. The (100) mirror plane (m) is shown.

In spite of orientation disorder the anions exhibit considerable thermal motion which gives rise to atomic displacement parameters of oxygen atoms. The disorder and large thermal motion of the anions in the phase III are probably the result of the lack of strong directional bonding and large volume available in the structure.

$[(CH_3)_3C_5H_2NH]^+$ rings lie on (012) and (0 − 12) lattice planes. The ring atoms deviate only slightly from least-square plane (the maximum deviation equals to 0.005(2)Å). C(21)H_3 methyl groups are slightly below the plane (the deviation equals to 0.018(4)Å). Methyl C(41) atoms lie on the mirror plane so that the hydrogen atoms are distributed over two symmetrically related sites (x,y,z and $2-x,y,z$). The cations seem to be strongly stabilized in the crystal structure as far as any distortions appear at temperatures ranging from 245 to 344K. Fig. 8 illustrates the most important details of molecular crystal packing of the III phase at 245K.

The $[(CH_3)_3C_5H_2NH]^+$ cations form quite close contacts to perchlorate anion giving 3D network of hydrogen bonds in the structure. Each cation is hydrogen bonded to $[ClO_4]^-$ via N(1)–H(1)···O(4) hydrogen bond with donor–acceptor distance of 2.912(2)Å, and the angle ∠ (DHA) of 155.6(8)°. It also interacts weakly with ring carbon and methyl groups via short C–H···O contacts, see Table 2. in supplementary materials. The hydrogen bonds are not strong enough to stabilize disordered $[ClO_4]^-$ anion. Consequently, the 3D array changes dynamically.

4.4. Low temperature superstructure, phase IV

III→IV PT results in 4*b* superstructure of phase III and symmetry change to $Pbn2_1$. Asymmetric unit grows to two independent cations TMPa and TMPb and two independent anions PR1 and PR2. The symmetry of $[ClO_4]^-$ and $[(CH_3)_3C_5H_2NH]^+$ lowers to C_1. The vanishing of the mirror plane leads to deformation of $[(CH_3)_3C_5H_2NH]^+$ arrangement. Cations are turned around axes that are perpendicular to their ring planes ([0−21] or [021]). However, the distortion from high temperature position differs for both ions.

At 210K the main axis N(1)–C(4) in TMPa deviates only slightly from (100) plane (1.24(5)°) whereas in TMPb about 5.07(3)°. Methyl C(41A)H_3 is almost collinear with N(1)–C(4) whereas C(41B)H_3 group is shifted by 0.022(2)Å from this direction. The distortion grows with temperature decrease. At 180K the N(1)–C(4) axis in TMPa cation leans out of (100) plane about 1.35(4)° whereas the TMPb about 5.75(2)°.

In the unit cell the mean deviation of N–C(4) axis from (100) plane is equal to zero since both TMPa and TMPb $[(CH_3)_3C_5H_2NH]^+$ cations lean out in [100] as well as [−100] direction. Fig. 9 illustrates the molecular structure and cations distortions at 180K. Atom numbering scheme as well as crystal packing at 180K are available in supplementary materials in Figs. 17 and 18.

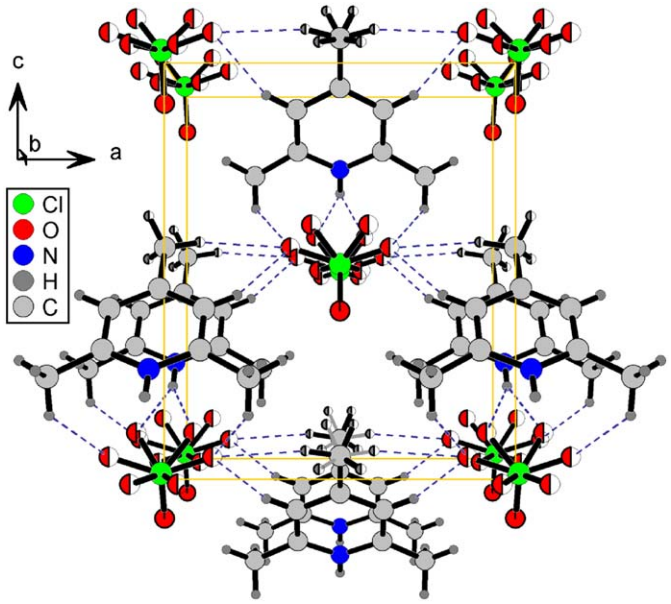

Fig. 8. The crystal packing in phase III, $T = 245$ K. The half-atoms illustrate the orientational disorder of perchlorate anions.

Modification of cationic substructure affects the dynamics of the $[ClO_4]^-$ anions. The perchlorate PR1 bonded to TMPa is in the IV phase still disordered over two positions, in 3:2 ratio, and interacts with TMPa via N(1A)–H(1A)···O(13) with the donor–acceptor distance of 2.843(3)Å or N(1A)–H(1A)···O(13A) of 2.891(6)Å. On the other hand, the PR2 anion interacting with TMPb is ordered and bounds to TMPb via N(1B)–H(1B)···O(23) of 2.895(3)Å. Together with the changes of $[(CH_3)_3C_5H_2NH]^+$ and $[ClO_4]^-$ arrangement additional C–H···O contacts appear, see Table 2.

4.5. Low temperature phase V

Order–disorder process of the $[ClO_4]^-$ groups and displacement of $[(CH_3)_3C_5H_2NH]^+$ cations is finalized in an arrangement of the low temperature phase. The IV→V PT implies an ordering of the perchlorate as well as further displacements of the ring atoms leading in particular to symmetry decrease to monoclinic one, and the space group *Pn* that allows the polar axis to arise in (a,c) plane. Elementary cell shrinks again to the dimensions from the III phase, and an independent cell to the one perchlorate and one $[(CH_3)_3C_5H_2NH]^+$ cation. The $[ClO_4]^-$ is fully ordered and seems to be strongly stabilized via N(1)–H(1)···O(4) hydrogen bond of 2.873(3)Å. All the cations in the unit cell incline in one direction, giving the distortion of N(1)–C(4) axis from (001) plane of 6.721°. The changes result in a slight decrease in the *a* lattice parameter. Simultaneously, the increase of the dihedral angle between the cations, from 86.42(3)° at 180K to 88.87(6)° at 115K results in a distinct increase of *b* parameter. Fig. 10 illustrates the most important details of molecular packing at 115K.

5. Pyroelectric measurements

In order to confirm the polar character of $[(CH_3)_3C_5H_2NH][ClO_4]$ the pyroelectric measurements were carried out in the wide temperature range. Fig. 11 presents the pyroelectric current and the change in the spontaneous polarization (ΔP_s) vs. temperature

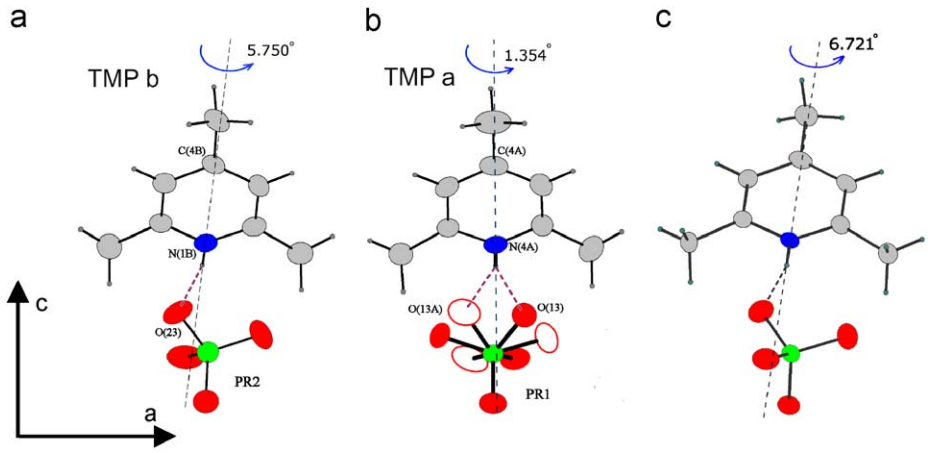

Fig. 9. The molecular structure of $[(CH_3)_3C_5H_2NH][ClO_4]$ in phases IV and V, (a,b) 180K and (c) 115K.

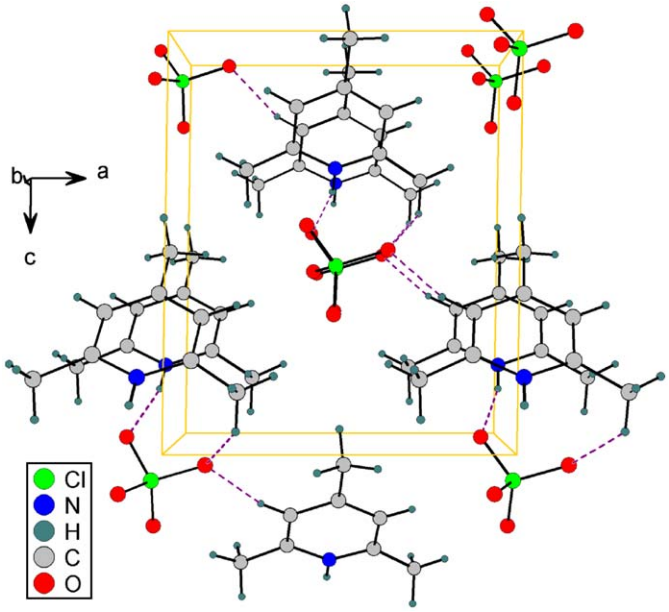

Fig. 10. The crystal packing of $[(CH_3)_3C_5H_2NH][ClO_4]$ in phase V, 115K.

in the vicinity of III→IV and IV→V phase transitions on cooling and heating. The spontaneous polarization (ΔP_s) changes at both low temperature phase transitions. ΔP_s of III↔IV PT is of the order of $1\times10^{-4}\,C/m^2$. During this phase transition temperature hysteresis is not observed and the value of ΔP_s does not depend on the direction of the run. ΔP_s of IV→V PT amounts to $1.5\times10^{-3}C/m^2$ on cooling and 1×10^{-3} on heating. This behavior is well reproducible: does not depend on the sample history. It is worth to emphasize that P_s reaches the value that is encountered for "weak" ferroelectrics e.g. A_2BX_4-type family of incommensurate crystals [36].

The pyroelectric current measurements were carried out in the high temperature region as well. Their results are presented in Fig. 12. On heating the high peak associated with the current flow is observed at the II→I phase transition temperature. The change in the spontaneous polarization amounts to $8\times10^{-3}\,C/m^2$. It should be noted that entering the phase II is manifested only by small noise of current and, most probably, is associated with whitening (partial powdering) of the crystal. On cooling the pyroelectric effect is also observed but the current and the ΔP_s reach much smaller values than those on heating. It must be also the effect of sample powdering.

In order to verify the possible ferroelectric properties in $[(CH_3)_3C_5H_2NH][ClO_4]$ crystals the set of experiments with applying the bias electric field was performed. First, the spontaneous polarization direction was attempted to be reversed close to I→II phase transition. The procedure of performing this experiment is as follows. The sample is heated up from room temperature (phase III) to 370K (phase I) and in this phase the bias electric field is applied. Next the sample is cooled down back to phase III, the bias electric field is switched off and the sample is heated up again to phase I and the pyroelectric current is recorded. Then the bias electric field of the opposite direction is applied, crystal is cooled down again through phase transition and starting from phase III next measurement is carried out. If the compound is ferroelectric and the applied external field exceeds the coercive field of the crystal one may observe the reversed spontaneous polarization. In the case of $[(CH_3)_3C_5H_2NH][ClO_4]$ in phase I each sample exhibited very high conductivity with a high voltage applied thus the expected pyroelectric current was masked by the ionic/defects contribution. The high conductivity was most probably caused by crystal defects induced by powdering of the sample.

Similar procedure was applied for studying the IV→V phase transition. The crystal was heated up as close as possible the III→II phase transition without reaching it. In this way one avoids whitening of the sample and minimizes the coercive field which diminishes approaching the T_c. Then the bias electric field was applied and the sample was cooled down through phases III and IV to phase V. The electric field was switched off, the sample was short circuited for 30min and then heating scan was recorded. The results of these measurements are presented in Fig. 13. One can see that the values of ΔP_s are quite markedly different from each other but the direction of the P_s was not reversed. It concludes that $[(CH_3)_3C_5H_2NH][ClO_4]$ is a strong polar/pyroelectric material over the phases III, IV and V what is in agreement with the X-ray studies. Moreover, it may be said that $[(CH_3)_3C_5H_2NH][ClO_4]$ is potential ferroelectric material with extremely high coercive field.

6. Dielectric studies

The dielectric measurements were performed in a wide temperature range encompassing all the phase transitions

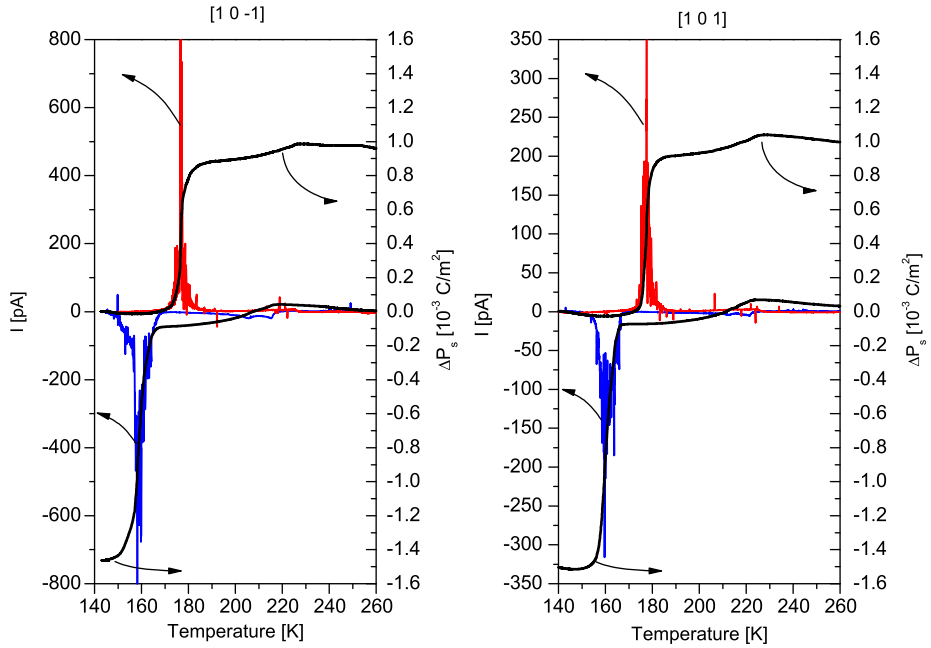

Fig. 11. The pyroelectric current and the change of the P_s measured along [10−1] and [101] directions.

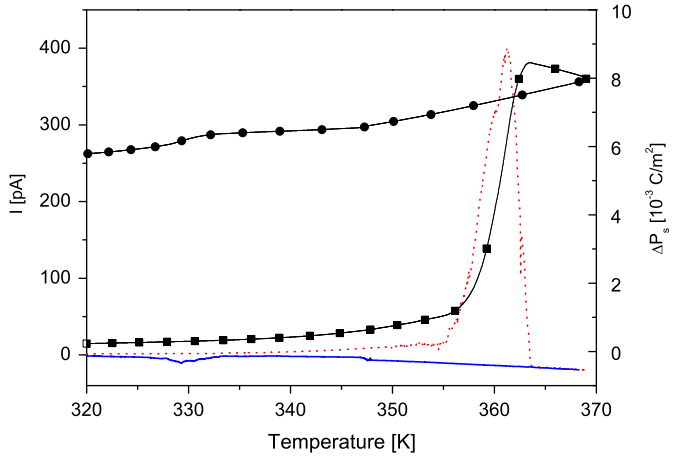

Fig. 12. The pyroelectric current (dotted/solid line for heating/cooling) and the change of the P_s (squares/circles) measured along [10−1] in the high temperature range.

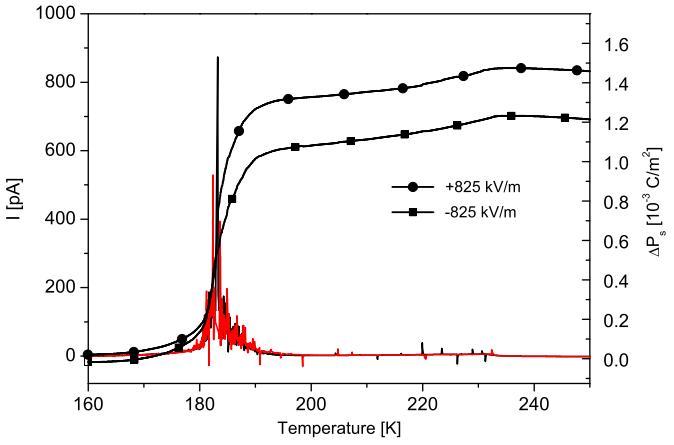

Fig. 13. The pyroelectric current (solid lines) and the change of the P_s measured along [10−1] with bias electric field ±825 kV/m (circles/squares).

found in $[(CH_3)_3C_5H_2NH][ClO_4]$. The results are presented in Fig. 14.

The single crystal X-ray studies showed that $[(CH_3)_3C_5H_2NH][ClO_4]$ crystallizes in the piezoelectric/polar space group ($Pmn2_1$). The piezoelectric properties are reflected in the dielectric response as a so-called resonance response (see the electric permittivity vs. temperature curve measured at the frequency of 300kHz in Fig. 14(a)). The III→IV phase transition dielectric anomaly is hardly visible whereas the IV→V phase transition is manifested as a little increase in the electric permittivity value.

Although in the high temperature range the dielectric anomalies associated with phase transformations are much more drastic than at low temperatures, the conductivity strongly modifies electric response of the $[(CH_3)_3C_5H_2NH][ClO_4]$ crystal. It may be caused by the mechanical instability (whitening) of the sample. However, it is clear that the III→II phase transition is connected with a step-wise increase of ε' values and step-wise decrease at the II→I transition point. Despite the powdering of the sample the phase transition is reversible and on cooling is manifested as a sharp peak with characteristic temperature hysteresis.

7. Discussion

The $[(CH_3)_3C_5H_2NH][ClO_4]$ crystal is characterized by a rich variety of solid–solid state phase transitions. The phase relations can be summarized as follows:

The mechanism of the low temperature phase transitions seems to be quite clear. Basing on the X-ray studies on the phases III, IV and V one may conclude that both $[ClO_4]^-$ anions and $[(CH_3)_3C_5H_2NH]^+$ cations (TMP) play equal role in the III→IV and IV→V phase transformations. Anionic and cationic moieties, respectively, are responsible for the order–disorder and displacive contributions to these phase transitions mechanism.

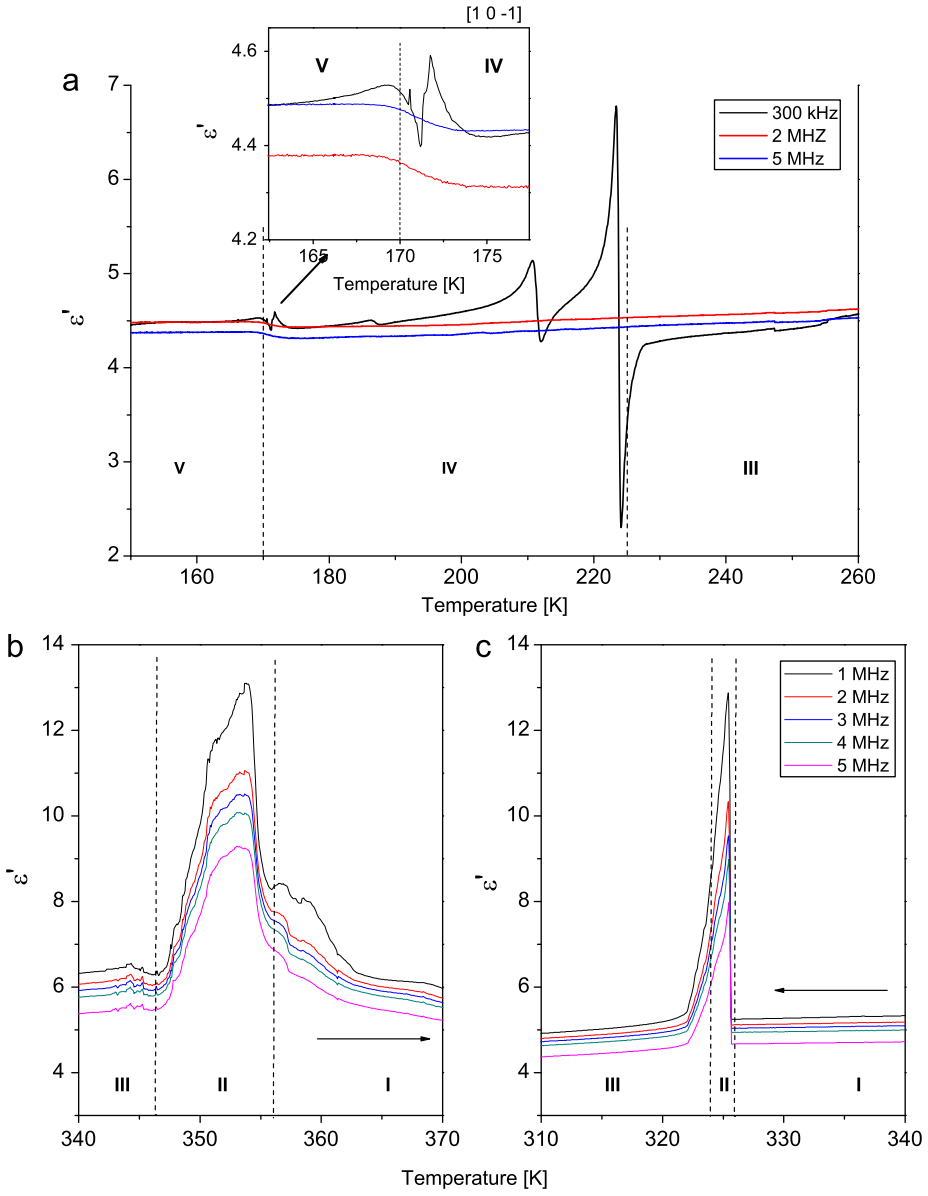

Fig. 14. The electric permittivity vs. temperature in the low temperature region on cooling (a); high temperature region on heating (b) and cooling (c).

In the phase III all $[ClO_4]^-$ are distributed over two sites with an

$$\begin{array}{ccccccc}
 & \overset{170}{\underset{182}{}} & & \overset{226}{} & & \overset{326}{\underset{346}{}} \quad \overset{327}{\underset{356}{}} & & \overset{\text{cooling}}{\underset{\text{heating}}{}}\,\mathrm{T[K]} \\
\xrightarrow[(V)]{Pn} & | & \xrightarrow[(IV)]{Pbn2_1} & | & \xrightarrow[(III)]{Pmn2_1} & | & \xrightarrow[(II)]{?} \quad | \quad \xrightarrow[(I)]{P222\ or\ Pmmm} \\
 & 1.5\cdot 10^{-3} & & 1\cdot 10^{-4} & & 0 \quad 8\cdot 10^{-3} & & \Delta P_s[C/m^2] \\
 & \underbrace{\qquad\qquad\qquad\qquad\qquad\qquad\qquad\qquad\qquad\qquad}_{polar} & & & & \underbrace{\qquad\qquad}_{non-polar} &
\end{array}$$

equal probability. The III→IV PT at 226K of the second order type involves significant changes in the dynamics of the anionic substructure. One part of anions becomes ordered whereas the other part remains disordered (two-site model with nonequivalent positions). The expected value of ΔS_{tr} should be ca. $\frac{1}{2}R\ln 2 = 2.88\,\mathrm{J\,mol^{-1}\,K^{-1}}$ but for second-order transitions the DSC method does not allow us to verify it directly. The further change in the dynamic of anions takes place at 170K when crystal undergoes IV→V PT. In the phase V all anions become fully ordered. ΔS_{tr} accompanying the IV→V transition was found to be

ca. 1.3 J mol^{-1} K^{-1}, which is distinctly smaller than expected value for the two-site model for half amount of cations ($\frac{1}{2}R\ln 2 = 2.88$ J mol^{-1} K^{-1}). This difference may suggest that disordered cations in the phase IV are distributed between two sites with significantly various occupations and one of these occupation becomes favored approaching 170K (at 180K the ratio of ordered to disordered anions is 3:2). Nevertheless, taking into account the total change in the dynamical state of anions covering two PTs (III→IV and IV→V) full amount of the transition entropy should be $R\ln 2 = 5.88$ J mol^{-1} K^{-1}, which confirms univocally that the higher temperature PT at 226K is dominated by the order–disorder mechanism. Changes in the mutual orientation of $[(CH_3)_3C_5H_2NH]^+$ may be considered as a displacive contribution to the mechanism of III→IV and IV→V phase transitions (see Fig. 9).

In the high temperature region the analysis of phase situation is more complicated because of weak mechanical stability of the compound. The phase transition III→II is accompanied by a powdering/disintegration of the samples, thus these transitions are practically irreversible in the dilatometric and, especially, in pyroelectric measurements which are sensitive to mechanical defects. The large magnitudes of ΔS_{tr}: 10.3 J mol^{-1} K^{-1} ($R\ln 3.5$) and 21.5 J mol^{-1} K^{-1} ($R\ln 13$) for the (III→II) and (II→I) PT, respectively, indicate a significant changes in the dynamics of the $[ClO_4]^-$ anions and TMP cations due to these transformations. The former transformation may be explained in terms of freedom of motion of $[ClO_4]^-$ anions, which is expected to increase significantly. The highest temperature transition, characterized by an enormous ΔS_{tr} value, should involve dynamics of both anions and cations.

At low temperature region the crystal X-ray studies show that the IV→V PT is the paraelastic–ferroelastic type ($mm2 \rightarrow m$). In the case of $[(CH_3)_3C_5H_2NH][ClO_4]$ the ferroelastic distortion is most likely due to the shift of the molecules within the cation substructure. Although the attempt to visualize the ferroelastic domain structure was performed, it was not successful. Most probably the domains were either too tiny or an application of an external stress was necessary to induce them. Such a situation took place in the case of e.g. $[(4-CNC_5H_4NH)][ClO_4]\cdot H_2O$ [31] or $Pb_3(PO_4)_2$ [37] which undergo the paraelastic–ferroelastic transition of an improper type.

The most interesting feature of $[(CH_3)_3C_5H_2NH][ClO_4]$ appears to be its polar properties found over a wide temperature region, including the room temperature phase, which is beneficial from an application point of view. The X-ray studies show that $[(CH_3)_3C_5H_2NH][ClO_4]$ crystallizes in the polar space group $Pmn2_1$ (phase III, room temperature). The polarity of this phase is due to the arrangement of the dipole moments assigned to the trimethylpyridinium cations (TMP). TMP dipole moments lie in [021] and [0−21] directions only the projection on *c*-axis gives the contribution to total dipole moment of the unit cell. In the case of the *mm*2 point group the polar twofold axis coincides with the *c* direction, which was confirmed by the present pyroelectric measurements.

To characterize the polar properties of $[(CH_3)_3C_5H_2NH][ClO_4]$ we should discuss the evolution of the spontaneous polarization with temperature in the successive phases. Fig. 15 shows schematically the change in the orientation of TMP cations and corresponding changes of spontaneous polarization. The transformation from the phases III to IV is related to deviation of N(1)–C(4) axis from the (100) plane (see Section 4.4) therefore the subtle step-wise increase of ΔP_s is observed at 226K. The further decreasing of temperature over phase IV leads to bigger deflection of $[(CH_3)_3C_5H_2NH]^+$ and by the fact itself small decay of polarization (see Fig. 11). This arrangement of TMP entails change of P_s only along *c*-axis but this situation changes entering the phase V. In the lowest temperature phase all cations lean out in the same direction over 6° what causes further decrease of polarization along *c*-axis and appearance of the P_s component in the *a* direction. The resultant vector of polarization lies in the (101) plane.

The change of the spontaneous polarization in the high temperature region seems to be caused by a quite drastic modification of the cationic substructure. As far as the phase transition III→II does not affect the magnitude of P_s, the II→I PT is related with significant change of P_s. It confirms the conclusion drawn from calorimetric measurements that the $[(CH_3)_3C_5H_2NH][ClO_4]$ in phase I is characterized by change of dynamical state of cations. Basing on the powder X-ray measurements we cannot unambiguously choose the point group of the highest temperature phase, but the magnitude of the ΔP_s may suggest centrosymmetric or at least non-polar space group (*mmm* or 222, respectively).

Despite the fact that the pyroelectric measurements allows us to estimate only the changes in the spontaneous polarization (ΔP_s) near the phase transition temperatures, we should emphasized that changes in P_s close to I→II (8×10^{-3} C/m^2) and IV→V (1.5×10^{-3} C/m^2) significantly exceed those observed for typical pyroelectric materials and characteristic of "weak" ferroelectrics crystals, i.e. the crystals with a weakly polar soft mode [38–41]. On the other hand we could not confirm the reversibility of the spontaneous polarization starting from the phase II. The powdering of the single crystal sample did not enable us to apply dc electric field strong enough to reverse the spontaneous polarization (to overcome the coercive field). Nonetheless, results of dielectric measurements seem to confirm the possible ferroelectricity in the $[(CH_3)_3C_5H_2NH][ClO_4]$ crystal:

- in the high temperature region the dielectric response which is seen as a strong dielectric anomaly with rather small increment is characteristic of "weak" ferroelectrics [38,39];
- in the low temperature region, close to III→IV and IV→V phase transitions, dielectric anomalies are rather weak and characteristic of "improper" structural phase transitions (ferroelectric–ferroelectric type?). It was shown that the III→IV transition is accompanied by a fourfold increase of the *b* lattice constant (4*b* superstructure of phase II), whereas the IV→V transition leads to a fourfold decrease of this parameter.

Moreover, it should be underlined that the most intriguing pyroelectric feature is the fact that we could observe a

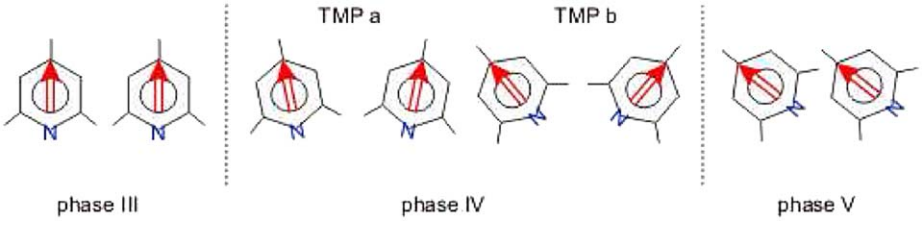

Fig. 15. The schematic arrangement of TMP molecules in phases III, IV, and V. The arrows stand for dipole moment.

real influence of the bias dc electric field on the value of P_s in the phase V (see Fig. 13). It may reflect the presence of the ferroelectric domain structure in the successive phases at low temperatures.

8. Conclusions

1. The compound reveals a rich polymorphism in the solid state. It undergoes four solid–solid phase transitions: from phases I to II at 356/327K (heating–cooling), II→III at 346/326, III→IV at 226K and IV→V at 182/170K.
2. $[(CH_3)_3C_5H_2NH][ClO_4]$ in the room temperature phase III crystallizes in the polar space group ($Pmn2_1$) and the polar properties are maintained in the successive phases: IV ($Pbn2_1$) and V (Pn).
3. The polar properties and evolution of the P_s with temperature of $[(CH_3)_3C_5H_2NH][ClO_4]$ are due to mutual orientation of the dipolar TMP cations.
4. The strong pyroelectric effect is one of the important features of the title crystal. The spontaneous polarization changes, ΔP_s, over the phases V–II, ranges from 1.5 to 8×10^{-3} C/m^2, which is characteristic of a weak ferroelectric materials.
5. The spontaneous polarization was found to be irreversible in the polar phases, however, there could be observed a noticeable influence of the bias electric field on the P_s magnitude in the vicinity of the IV→V PT which may reflect the presence of the ferroelectric domain structure at low temperatures.

Appendix A. Supporting information

CCDC 720203-720209 contains the supplementary crystallographic data for this paper. These data can be obtained free of charge via www.ccdc.cam.ac.uk \data_request\cif, or by emailing data_request@ccdc.cam.ac.uk, or by contacting The Cambridge Crystallographic Data Centre, 12, Union Road, Cambridge CB2 1EZ, UK; fax: +44 1223 336033.

Appendix B. Supplementary data

Supplementary data associated with this article can be found in the online version at 10.1016/j.jssc.2009.07.055.

References

[1] Z.L. Wang, Z.C. Kang, Functional and Smart Materials: Structural Evolution and Structure Analysis, Plenum Press, New York, 1998.
[2] G.R. Desiraju, Crystal Engineering: The Design of Organic Solids, Elsevier, New York, 1989.
[3] J. Zyss, Molecular Nonlinear Optics: Materials, Physics and Devices, Academic Press, New York, 1993.
[4] F. Agullo-Lopez, J.M. Cabrera, F. Agullo-Rueda, Electrooptics: Phenomena, Materials and Applications, Academic Press, New York, 1994.
[5] J.-L. Lehn, Supramolecular Chemistry: Concepts and Perspectives, VCH Publishers, New York, 1995.
[6] T.J. Marks, M.A. Ratner, Angew. Chem. 107 (1995) 167.
[7] T.J. Marks, M.A. Ratner, Angew. Chem. Int. Ed. Engl. 34 (1995) 155.
[8] R.-G. Xiong, X.-Z. You, Inorg. Chem. Commun. 5 (2002) 677.
[9] J.C. Evans, Spectrochim. Acta 16 (1960) 428.
[10] M.S. Wong, C. Bosshard, P. Gunter, Adv. Mater. 9 (1997) 837.
[11] H. Zhang, X.M. Wang, K.C. Zhang, B.K. Teo, Coord. Chem. Rev. 183 (1999) 157 (and references therein).
[12] V.R. Thallad, S. Brasselet, H.C. Weiss, D. Blaser, A.K. Katz, H.L. Carrell, R. Boese, J. Zyss, A. Nangia, G.R. Desiraju, J. Am. Chem. Soc. 120 (1998) 2563.
[13] M. Ohkita, T. Suzuki, K. Nakatan, T. Tsuji, Chem. Commun. (2001) 1454.
[14] K.T. Holman, A.M. Pivovar, M.D. Ward, Science 294 (2001) 1907.
[15] G.R. Desiraju, Nature 412 (2001) 397.
[16] O.M. Yaghi, C.E. Davis, G.M. Li, H.L. Li, J. Am. Chem. Soc. 119 (1997) 2861.
[17] P.A. Maggard, C.L. Stern, K.R. Poeppelmeier, J. Am. Chem. Soc. 123 (2001) 7742.
[18] H.N. Lee, D. Hesse, N. Zakharov, U. Gosele, Science 296 (2002) 2006.
[19] G. Xu, G.-G. Guo, M.-S. Wang, Z.-J. Zhang, W.-T. Chen, J.-S. Huang, Angew. Chem. Int. Ed. 46 (2007) 3249.
[20] Q. Ye, D.-W. Fu, H. Tian, R.-G. Xiong, P.W.H. Chan, S.D. Huang, Inorg. Chem. 47 (3) (2008) 772–774.
[21] Z.-G. Gu, X.-H. Zhou, Y.-B. Jin, R.-G. Xiong, J.-L. Zuo, X.-Z. You, Inorg. Chem. 46 (14) (2007) 5462–5464.
[22] M.R. Bauer, C.R. Ross, R.M. Nielson, S.C. Abrahams, Inorg. Chem. 38 (5) (1999) 1028–1030.
[23] H. Zhao, Z.-R. Qu, Q. Ye, B.F. Abrahams, Y.-P. Wang, Z.-G. Liu, Z. Xue, R.-G. Xiong, X.-Z. You, Chem. Mater. 15 (22) (2003) 4166–4168.
[24] D.-W. Fu, W. Zhang, R.-G. Xiong, Cryst. Growth Des. 8 (9) (2008) 3461–3464.
[25] Z. Pająk, P. Czarnecki, H. Małuszyński, B. Szafrańska, M. Szafran, J. Chem. Phys. 113 (2000) 848–853.
[26] Z. Pająk, P. Czarnecki, B. Szafrańska, H. Małuszyńska, Z. Fojud, Phys. Rev. B 69 (2004) 132102–132104.
[27] Z. Pająk, P. Czarnecki, B. Szafrańska, H. Małuszyńska, Z. Fojud, J. Chem. Phys. 124 (2006) 144502.
[28] O. Czupiński, G. Bator, Z. Ciunik, R. Jakubas, W. Medycki, J. Świergiel, J. Phys. Condens. Matter 14 (2002) 8497–8512.
[29] O. Czupiński, R. Jakubas, A. Pietraszko, J. Mol. Struct. 704 (2004) 177–187.
[30] O. Czupiński, M. Wojtaś, J. Zaleski, R. Jakubas, W. Medycki, J. Phys. Condens. Matter 18 (2006) 3307–3324.
[31] O. Czupiński, M. Wojtaś, A. Pietraszko, R. Jakubas, Solid State Sci. 9 (2007) 108–115.
[32] M. Mayer, CrysAlis Programs for Data Collection and Reduction, Version 1.170.32, Oxford Diffraction Ltd, 2007.
[33] G.M. Sheldrick, Acta Cryst. A 64 (2008) 112–122.
[34] O. Czupiński, M. Wojtas, Z. Ciunik, R. Jakubas, Solid State Sci. (2006) 86–96.
[35] O. Czupiński, G. Bator, Z. Ciunik, R. Jakubas, Z. Medycki, J. Świergiel, J. Phys. Condens. Matter 14 (2002) 8497–8512.
[36] S. Sawada, M. Takashige, F. Shimizu, H. Suzuki, T. Yamaguchi, Ferroelectrics 169 (1) (1995) 207–214.
[37] Y.C. Cho, H.J. Lee, S.E. Park, C.R. Cho, S.-Y. Jeong, Phys. Rev. B 66 (18) (2002) 184103.
[38] F. Smutny, J. Fousek, Phys. Status Solidi 40 (1970) K13.
[39] D. Blum, J.C. Peuzin, J. Henry, Feroelectrics 69 (1984) 283.
[40] G. Smolenskij, I.G. Sinij, A.K. Tagantsev, S.D. Prokhorova, V.D. Mikvabiya, V. Vindsh, Zh. Eksp. Teor. Fiz. 88 (1985) 1020;
G. Smolenskij, I.G. Sinij, A.K. Tagantsev, S.D. Prokhorova, V.D. Mikvabiya, V. Vindsh, Sov. Phys. JETP 61 (1985) 599.
[41] A.K. Tagantsev, Zh. Eksp. Teor. Fiz. 45 (1987) 352;
A.K. Tagantsev, JETP Lett. 45 (1985) 44.